HHS Public Access

Author manuscript

Pediatr Res. Author manuscript; available in PMC 2021 June 01.

Published in final edited form as:

Pediatr Res. 2021 March ; 89(4): 838–845. doi:10.1038/s41390-020-1010-7.

Impairment in Neurocognitive Function Following Experimental Neonatal Guinea Pig Cytomegalovirus Infection

Claudia Fernández-Alarcón[1], **Lucy E. Meyer**[1], **Michael A. McVoy**[2], **James R. Lokensgard**[3], **Shuxian Hu**[3], **Michael A. Benneyworth**[4], **Kaitlyn M. Anderholm**[1], **Bradley C. Janus**[1], **Mark R. Schleiss**[1,*]

[1]Department of Pediatrics, University of Minnesota Medical School, Minneapolis, Minnesota

[2]Department of Pediatrics, Virginia Commonwealth University School of Medicine, Richmond, Virginia

[3]Department of Medicine, Neurovirology Laboratory, University of Minnesota Medical School, Minneapolis, Minnesota

[4]Mouse Behavior Core, University of Minnesota, Minneapolis, Minnesota

Abstract

BACKGROUND: Cytomegalovirus (CMV) is a leading infectious cause of neurologic deficits, both in the settings of congenital and perinatal infection, but few animal models exist to study neurodevelopmental outcomes. This study examined the impact of neonatal guinea pig CMV (GPCMV) infection on spatial learning and memory in a Morris water maze (MWM) model.

METHODS: Newborn pups were challenged intraperitoneally (ip) with a pathogenic red fluorescent protein (RFP)-tagged GPCMV, or sham-inoculated. On days 15–19 post-infection (pi), pups were tested in the MWM. Viral loads were measured in blood and tissue by quantitative PCR (qPCR), and brain samples collected at necropsy were examined by histology and immunohistochemistry.

RESULTS: Viremia (DNAemia) was detected at day 3 pi in 7/8 challenged animals. End-organ dissemination was observed, by qPCR, in lung, liver, and spleen. $CD4^+$ and $CD8^+$ T-cell infiltrates were present in brains of challenged animals, particularly in periventricular and hippocampal regions. Reactive gliosis and microglial nodules were observed. Statistically significant spatial

*Corresponding Author: Mark R. Schleiss, MD, University of Minnesota Medical School, MTRF, 2001 6th Street SE, Minneapolis, MN 55455, schleiss@umn.edu, Phone: 612-626-9913, Fax: 612-626-9924.

Author Contributions:

•Substantial contributions to conception and design, acquisition of data, or analysis and interpretation of data; CFA, LEM, MAM, JRL, SH, MAB, KMA, BCJ, MRS

•Drafting the article or revising it critically for important intellectual content; CFA, LEM, MAM, JRL, SH, MAB, KMA, MRS

•Final approval of the version to be published; CFA, LEM, MAM, JRL, SH, MAB, KMA, BCJ, MRS

Disclosure Statement: No Conflicts of Interest.

Category of Study: Basic Science Article.

Statement Regarding Patient Consent: Patient consent was not required for this paper (no patient subject matter or content).

learning and memory deficits were observed by MWM, particularly for total maze distance travelled ($p<0.0001$).

CONCLUSION: Neonatal GPCMV infection in guinea pigs results in cognitive defects demonstrable by the MWM. This neonatal guinea pig challenge model can be exploited for studying antiviral interventions.

INTRODUCTION

Human cytomegalovirus (HCMV) is a common congenital viral infection known to damage to the neonatal central nervous system (CNS). CNS manifestations in newborns can include microcephaly, cerebellar atrophy, polymicrogyria, ventriculomegaly, periventricular calcifications, focal necrosis, lissencephaly, and sensorineural hearing loss (SNHL; 1-4). Long-term neurological sequelae are observed in 16.8–18.8% of children with congenital CMV (5). Recently, it has also been suggested that post-natally acquired CMV infections can produced long-term neurodevelopmental sequelae in very-low-birthweight premature infants (6, 7).

Little is known about the mechanisms of long-term neurologic injury following perinatal viral infections. Since human CMV cannot be studied in animals, rodent models of perinatal viral challenge have been described using species-specific CMVs, such as the guinea pig cytomegalovirus (GPCMV; 8, 9) and murine cytomegalovirus (MCMV; 10-13). Following ip MCMV inoculation of newborn mice, virus disseminates to the CNS, and infection is coupled with recruitment of immunocytes and expression of pro-inflammatory cytokines. Perinatal MCMV infection also results in long-term motor and sensory disabilities, including cerebellar pathology (12) and SNHL (14, 15). We therefore sought to extend these neuropathogenesis studies to a neonatal viral challenge model in the guinea pig.

The studies we describe in the current report used the Morris water maze (MWM) to examine memory and cognition following neonatal infection with GPCMV. There have been limited studies of the MWM in rodent models of infectious diseases. The MWM was first described in the context of hippocampal-dependent learning and memory in rats (16). Previous rodent MWM studies observed that damage to the striatum, basal forebrain, cerebellum and cerebral cortex disrupted spatial learning and maze performance (17). Armien *et al.* showed that mice latently infected with herpes simplex virus-1 demonstrated inflammation and neuronal loss, associated with severe spatial memory deficits (18). Buenz *et al.*, using C57BL/6J mice infected with Theiler's murine encephalomyelitis virus, showed that memory impairment correlated with hippocampal injury (19). Maze performance in guinea pigs is impaired after ethanol exposure (20, 21), prenatal iron deficiency (22, 23), and exposure to the pesticide chlorpyrifos (24). To our knowledge, the impact of viral CNS infection (in particular with CMV) on MWM performance has not been evaluated in guinea pigs. We therefore examined the neuropathogenesis of GPCMV infection, following neonatal challenge, using the MWM.

METHODS

Virus, cells, and animals

Cell culture amplification of clonal, BAC-derived viral stocks was carried out in guinea pig lung fibroblast cells (GPL, ATCC-CCL158) as previously described (25). Pups were challenged with a virulent, red fluorescent protein (RFP)-tagged variant of GPCMV, N13R10r129-RFP, a strain expressing TurboRFP635 (25, 26). Hartley neonatal guinea pigs born to dams purchased from Elm Hill Laboratories (Chelmsford, MA, USA) were inoculated ip within 72 hours post-delivery with 5×10^6 PFU of N13R10r129-RFP (8 pups), or sham-inoculated with an equal volume of PBS (6 pups). Approval was obtained from the UMN Institutional Animal Care and Use Committee.

Real-time quantitative PCR analysis (qPCR)

DNA was isolated and viral loads were determined by qPCR as previously described (25). DNA was extracted from either 100 μl citrated blood collected at 0, 3, 7, 14, 21, and 35 days post-challenge, or from 0.05 g of homogenized liver, lung, spleen or brain (as described below).

Histology and immunohistochemistry

Two sham-inoculated and seven GPCMV-challenged guinea pigs were necropsied at day 35 pi. One GPCMV-challenged guinea pig was necropsied on day 14 pi. Brain, liver and spleen tissues were fixed overnight with 4% paraformaldehyde. Tissue sections were stained with hematoxylin and eosin (H&E), mounted using Permount (Fisher), and examined by light microscopy. Immunofluorescence staining was performed as previously described (25). Supplemental Table S1 specifies the antibodies used in these experiments.

Morris water maze

Guinea pig pups were tested in the MWM beginning at day 15 pi. The rationale for selecting this time point was based on published data demonstrating resolution of guinea pig CNS infection by day 14 post-GPCMV challenge (27); hence, any neurocognitive abnormalities should represent sequelae of perinatal infection, and not be related to acute viremia/active infection of the CNS. Indeed, our data (described below in results section) demonstrated clearance of viremia by day 14. The MWM consisted of a circular (160 cm in diameter, 63.5 cm in height) metal tank filled with water (approximately 42 cm deep, temperature 20–21 °C). The water was tinted black with the addition of nontoxic black latex paint. A hidden circular escape platform (20 cm in diameter, 40 cm in height) was placed in the center of one of the four tank quadrants, submerged approximately 2–3 cm. A visual cue (bright blue geometric shape on a white background) was placed on each of the four walls above the tank to adapt the guinea pigs to their surroundings.

All pups were tested for five consecutive days. The five days were divided into two phases: the acquisition phase (days 1–4), followed by the probe phase (day 5). During the acquisition phase, the escape platform remained in the same position in the tank, whereas during the probe phase, the escape platform was removed. Each animal was tested four times daily for a maximum of 90 s, or until the animal found the escape platform. To begin a trial,

the animal was placed into the maze facing the wall of the tank at a specified point. The entry point was changed between trials. The order of the entry point was the same for each animal in the group, but was pseudo-randomized among training days. Once the animal found the platform or was guided there, it stayed for 10–15 s to observe its surroundings. The animals were studied in groups of 5, and completed their entire day of training before the next 5 animals began. On the fifth day of testing the platform was removed and each animal completed one 60 s free swim. The path of each guinea pig was recorded by a Fire-i™ board video camera outfitted with a 2.1 mm lens (Unibrain, Inc., San Ramon, CA, USA) and movements analyzed using ANY-maze software (Version 4.70, Stoelting Co., Wood Dale, IL, USA). Recorded data included: 1) total distance traveled; 2) swim speed; 3) time to first target zone entry (escape latency); and 4) number of platform crossings. Data obtained during the acquisition phase was averaged across the four trials each day to quantify and compare the metrics of task acquisition/learning.

Statistical methods

Statistical analysis was performed using the Prism 6 software (GraphPad Software, Inc., La Jolla, CA, USA). Two-sample *t*-test comparisons were performed between the experimental groups at each data point sequentially, so there are multiple comparisons that were being made within a single dataset. The probe test was analyzed by quantifying platform crosses, a single number for each animal and group. Learning trials such as escape latency, swim speed, and distance were analyzed with one-way analysis of variance (ANOVA), with post-hoc *t*-tests correcting for multiple comparisons. Differences between the two groups during the singular probe test were analyzed by student's *t*-test. Pup weights were compared with Dunn's multiple comparisons.

RESULTS

Disseminated viral infection occurs, with clearance of DNAemia by day 14 following challenge with a virulent, RFP-tagged GPCMV

Stocks of a virulent, RFP-tagged GPCMV strain, N13R10r129-RFP, were generated as previously described (25, 26). Animal weights in sham-inoculated (6/6) and virus-challenged animals (8/8) were recorded daily as a measure of pathogenesis. Sham-inoculated animals showed significantly greater weight gain compared to GPCMV-challenged animals ($p<0.05$) (Figure 1a). Viral load analyses demonstrated that DNAemia was present in 7 of 8 challenged animals at day 3 pi and in 8/8 animals at day 7 (mean viral load, 1.4×10^4 GPCMV genome copies/ml of blood). At day 14 pi, one challenged animal was necropsied; this animal had a blood viral load of 7.9×10^6 GPCMV genome copies/ml. DNAemia cleared in the remaining challenged animals by day 35 pi (Figure 1b). To examine visceral viral load, tissues from the animal sacrificed at day 14 were harvested, and the seven remaining challenged animals (and two sham-inoculated animals, data not shown) were sacrificed at day 35 pi and viral load quantified in lung, liver, spleen and brain. Viral DNA was detected in the spleen (mean, 2.47×10^2 genomes/mg) and liver (mean, 4.9×10^1 genomes/mg) in 6 of 7 day 35-challenged animals, but less frequently in the lung (1 of 7, 1.3×10^1 genomes/mg). No viral DNA was identified in brain tissue in day 35 samples (Figure 1c), but DNA was detected in the day 14 brain sample (closed circle).

Immunoperoxidase staining with a GP83-specific rabbit monoclonal antibody (moab; 28) also identified GPCMV antigen in brain tissue (brown cells, Figure 1d). Immunostaining with neuronal nuclear protein (NeuN) and glial fibrillary acidic protein (GFAP) antibodies demonstrated co-localization with viral antigen (Figure 1d; yellow cells, white arrows), confirming *bona fide* infection of brain cells, and not simply leukocytic trafficking of antigen into brain. No RFP^+ cells were observed in animals sacrificed on day 35 pi (data not shown).

Visceral dissemination was also confirmed by visualization of N13R10r129-RFP positive cells (RFP^+) in tissue sections. RFP^+ cells (red cells) were observed in spleen and liver sections in a pup necropsied at day 14 pi. Supplemental Figure S1 demonstrates RFP fluorescence of N13R10r129-RFP positive cells (red cells, white arrow) in brain and liver sections. Supplemental Figure S2 demonstrates spleen sections: **a)** stained with a mouse anti-GPCMV gB 29.29 moab; **b)** unstained cryosection exhibiting RFP expression from GPCMV-positive cells and; **c, d)** merged images with counterstaining with DAPI at low and high magnification. Confocal fluorescence images demonstrated RFP+ (N13R10r129-RFP-infected) cells in brain sections from the animal necropsied at day 14 pi, and Z-stack images of RFP^+ cells were recorded, processed, and analyzed for 3-dimensional (3D) reconstruction (Supplemental Video S1). Fluorescence intensity in the 3D reconstitutions was quantified using IMARIS software (version 7.4). The fluorescence intensity of the red channel corresponded to infected cells expressing RFP, while the intensity of the blue channel reflected nuclear fluorescence (DAPI). Non-infected cell nuclei had higher mean fluorescence intensities (400 AU) compared to infected cells (200 AU; yellow arrow, Supplemental Figure S3).

Histopathological abnormalities in GPCMV-infected brain

Histological examinations of coronal brain sections from the challenged animals were compared to uninfected controls. Gross disruption of brain histology, including bilateral ventricular dilatation with reduced thickness of cerebral cortex, was observed in two animals (Figure 2a). We analyzed levels of NeuN immunoreactivity in damaged brains. In the challenged group, decreased NeuN staining was observed in the cerebral cortex and hippocampus, compared to controls where a high NeuN immunoreactivity was observed (Figure 2b, c).

Inflammation and reactive gliosis in GPCMV-infected pups

To investigate the nature of CNS inflammation following neonatal GPCMV challenge, immunohistochemical staining for CD4-positive ($CD4^+$) and CD8-positive ($CD8^+$) T lymphocyte cell markers was performed on brain sections. No $CD4^+$ or $CD8^+$ lymphocytes were observed in brains of sham-inoculated animals (Figure 3a). $CD4^+$ and $CD8^+$ T-cell infiltration were identified in all brains of GPCMV-challenged pups (8/8). Figure 3b demonstrates a representative coronal section from a brain collected at day 14 pi with inflammatory cell infiltrates localized in the cortical region (black arrows). By immunofluorescence staining, these cells were confirmed to be $CD8^+$ lymphocytes. The brain sections from the challenged animals collected at 35 days pi exhibited scattered inflammatory infiltrates localized in the periventricular and hippocampal regions. Focal

aggregates of T-lymphocytes were also identified in the thalamus, hypothalamus and third ventricle regions of these brains (Figure 3c).

We next examined the immunoreactivity of reactive astrocytes and activated microglia in brain sections using GFAP and ionizing calcium-binding adaptor molecule 1 (Iba1) abs, respectively. Immunostaining for GFAP revealed reactive astrogliosis in the brains of challenged guinea pigs, including the hippocampus and ventricular regions. The cell bodies of these astrocytes were enlarged, and their processes were thickened, and increased GFAP immunoreactivity was observed compared to sham-inoculated animals (Figures 4a-c). 3D reconstructions of astrocyte filaments were generated from confocal Z-stacks using Imaris (Bitplane). Dual staining sections for T-lymphocytes and astrocyte activation markers revealed that areas of increased inflammatory cell infiltration were associated with areas of reactive gliosis (Figure 4b, d). Evidence of astrocyte activation and persistent chronic inflammation around the hippocampus in N13R10r129-RFP challenged guinea pigs at 35 days pi is noted in Supplemental Figure S4, demonstrating brain sections double-stained for $GFAP^+$ (red cells) and $CD8^+$ inflammatory T-cells (green cells) and counterstained with DAPI, with strongly positive GFAP astrocytes with multiple elongated processes in challenged animals noted compared to controls. Scattered $CD8^+$ infiltrates were also observed (see also Supplemental Video S2 online). Dense accumulations of $GFAP^+$ end-feet and processes of reactive astrocytes wrapping around blood vessels were observed (Figure 4c and Supplemental Video S3 online). Figure 5 shows representative microscopic images of coronal brain sections stained with Iba1 antibody. Strongly staining cells with highly branched processes were observed in brain sections from five GPCMV-challenged animals, but not controls, suggesting that these immunopositive cells were activated microglia (Figure 5a, b). Moreover, microglial nodules were also observed throughout the brain in three guinea pigs in the challenged group (Figure 5c).

GPCMV infection impairs spatial learning and memory

In order to study the effect of neonatal GPCMV challenge on spatial learning and memory, guinea pigs challenged with N13R10r129-RFP (7/8, day 15 pi), and sham-inoculated animals (6/6), were tested using the MWM for 5 consecutive days using previously described methods (21–23). From days 1 to 4 of the experiment (acquisition phase), the escape platform remained in the same location in the pool, and on day 5 (probe phase) the platform was removed. On the last day of the acquisition phase there was a significant decrease in total distance traveled between the two groups: GPCMV-challenged animals swam an average of 11.7 m, compared to the 5.0 m traveled in sham-inoculated animals ($p<0.0001$ by one-way ANOVA, Figure 6a). A statistically significant increase in the time to find the hidden platform was noted (escape latency, a measure used as an early indicator of learning [22]) in the challenged compared to sham-inoculated animals ($p<0.001$ by one-way ANOVA, Figure 6b). During this phase, swim speed was also measured, and the sham-inoculated animals swam significantly faster than the challenged animals ($p<0.05$ by one-way ANOVA, Figure 6c). Overall, these results indicate that the challenged guinea pigs had more difficulty finding the hidden platform compared to controls. A representation of these results is observed in the occupancy plots in Figure 6d. On day 4 of training (final training day), the animals in the GPCMV-challenged group spent a significant amount of their time

exploring the maze and were unable to locate the platform, while the control animals quickly found their way to the platform.

After learning was complete, reference memory was assessed by measuring the number of passes over the target quadrant where the platform used to be. The challenged group performed fewer platform crosses than the sham-inoculated animals. During the first 30 seconds of the probe test, challenged animals crossed the target platform zone on average 0.86 times, compared to controls crossing 2.17 times ($p<0.05$ by unpaired t-test; Figure 6e). The lack of preference to the target quadrant seen in the challenged group is evidence of significant memory deficit, further demonstrated by occupancy plots (Figure 6d), where the challenged group displayed a fairly distributed search of all quadrants, whereas controls targeted their search to where the quadrant was previously located. Additionally, it is noteworthy that the search strategy employed by the virus-challenged groups was to swim around the periphery of the tank. This serial search strategy, looking for an escape, further demonstrates cognitive impairment, insofar as the animals failed to acquire a spatial strategy of search based upon visual cues in the maze.

DISCUSSION

Neurodevelopmental impairment, commonly including learning and memory deficits, has long been associated with perinatally-acquired herpesvirus infections, including CMV (1, 5). We sought to develop a small animal model to assess neurobehavioral sequelae resulting from experimental neonatal CMV infection, using the MWM. In the MWM, spatial learning and memory is evaluated by a decrease in time (latency) to find the hidden platform and a reduction in path length (distance) traveled to the platform. The MWM has proven useful in other rodent viral challenge models. Espinoza *et al.* demonstrated that intranasal respiratory syncytial virus infection in mice and rats can spread from the airways to the CNS, causing functional alterations in the brain and resulting in poor MWM performance (29). Impaired cognition using the MWM was also shown by Jurgens *et al.* in a study of 4–6-month-old male BALB/C mice following intranasal infection with live influenza virus (30). For MCMV, pregnant BALB/C mice were subjected to intra-placental inoculation of virus (1 μL, 1×10^6 PFU), and learning and memory of the offspring at 70-day-old were analyzed by MWM test, which demonstrated that the infected groups exhibited longer latency times and increased swimming distance compared to controls (31). Similar results were observed by Lokensgard *et al.*, who reported that MCMV infection induced long-term neurological deficits (examined used a dry-land Barnes maze) in spatial learning and memory following regulatory T-cell (Treg) depletion (32). In the current study, we extended previous studies of spatial learning and memory in guinea pigs (20–24, 33) to the study of GPCMV infection. We found that neonatal guinea pigs challenged with a virulent, RFP-tagged GPCMV demonstrated significant impairment in MWM test performance, providing evidence of impairment of learning and memory associated with perinatal viral CNS infection.

One potential limitation of our model is that we did not perform direct intracerebral inoculation to unequivocally ensure CNS infection in all animals. Booss *et al.* inoculated young guinea pig intracerebrally (ic) with GPCMV (34). These authors reported that after ic inoculation with $10^{3.5}$ $TCID_{50}$ of GPCMV, levels of virus were found to peak in the brain

during the first week post-infection, and were reduced or cleared by week 3 or 4 pi. Glial nodule encephalitis was described in this direct CNS inoculation model. Other studies, however, have demonstrated that brain infection with GPCMV does not require direct intracerebral inoculation, and that extension of GPCMV infection to the CNS can occur following systemic routes of infection, both in pregnant (with subsequent infection of the fetus) and non-pregnant animals (9, 27, 35). A hematogenous route of seeding of the CNS, as opposed to a direct inoculation route, is more likely to recapitulate the pathology of brain infection in newborn infants with perinatally acquired CMV infections. Bravo *et al.* described a neonatal GPCMV challenge model, with viral dissemination to multiple organs, including brain, by day 10 post-challenge (9). Griffith *et al.* described brain and visceral infection in the context of congenitally-transmitted CMV infection in guinea pigs (35), and showed that GPCMV was recovered in cell cultures from salivary glands (18/24) and the spleen (8/24), but less commonly in brain (1/24).

In the current study, we used qPCR analysis to demonstrate that, after ip inoculation, high viral loads were detected in all organs, including brain from an animal that was necropsied at day 14 pi. In this challenge model, viremia essentially cleared after day 14. Growth velocities were also similar in infected and control groups after this day 14-time point, concomitant with the clearance of viremia (Figure 1a). Although evidence of active viral infection in the CNS was observed in one animal necropsied at day 14 (as evidenced by PCR and viral antigen expression), no evidence of active viral replication was present in the brains at the time of necropsy of other challenged animals at day 35. These findings are compatible with the observations made by Booss and colleagues, which indicated that GPCMV leptomeningitis and encephalitis had run their course and resolved by day 14 pi (34). MWW performance was assessed in our study beginning on day 15 pi, minimizing any concern that impaired MWM performance was due to an acute, symptomatic viremic illness.

Notably, both $CD4^+$ and $CD8^+$ T-cell infiltrates could be detected in brains from virus-challenged, but not sham-inoculated controls (Figure 3). Similar patterns of brain infection have been described with MCMV. Bantug *et al.* detected virus in the liver, spleen, and CNS following ip inoculation of neonatal BALB/c mice with MCMV (36), with virus peaking in the CNS between postnatal days 10–14. The activation of microglia we observed with Iba1 staining was of interest, given that CMV infection in human fetuses (20-to-29 weeks gestation) demonstrates a tropism for stem cells and radial glial cells, with concomitant focal microglial activation (2, 3). Although newborn mice are developmentally immature compared to newborn guinea pigs, our findings nonetheless suggest that GPCMV, similar to MCMV, disseminates to the CNS following neonatal challenge, eliciting histopathology and altered neurocognitive function. Based on MCMV studies, it is likely that eventual control of infection in the guinea pig CNS requires both a T-cell and a humoral immune response (13, 37, 38), although our observations demonstrate that neurocognitive sequelae occur even after clearance of infection is achieved.

Additionally, we postulate that neonatal brain damage induced by GPCMV in this model is not only due to virally-mediated damage to specific cell types, but also the attendant inflammatory response, which has been described in human fetal brain at the time of necropsy (2, 3). Gabrielli *et al.* demonstrated that in brains with severe cerebral damage,

microglial nodules included cytomegalic cells surrounded by activated $CD8^+$ T-lymphocytes and apoptotic cells (3). Observations in MCMV demonstrated chronic neuroinflammation, mediated by B cells, microglial cell activation, and retention of virus-specific memory $CD8^+$ T-cells, persisting in the absence of detectable viral antigens. IFN-γ secretion by brain-infiltrating T-cells contributed to microglial activation and tumor necrosis factor (TNF)-α production following MCMV infection of Fox3p-DTR-GRP mice, was exacerbated by Treg depletion, and was associated with reduced cognitive performance in spatial learning and memory tasks in the Barnes maze (32). We similarly noted that GPCMV-challenged guinea pigs demonstrated prominent reactive gliosis with inflammatory cell infiltrates, even in the absence of viral replication, at 35 days pi.

In summary, this is also to our knowledge the first functional assessment of memory and neurocognition in guinea pigs challenged with a neurotropic virus, GPCMV, utilizing the MWM. The MWM provides useful experimental endpoints to evaluate the impact of neonatal GPCMV infection and, potentially, antivirals and vaccines. The findings in this study provide evidence that neonatal infection in guinea pigs produces cognitive and learning defects, demonstrable histologically by immunostaining, and functionally by assessing performance in the MWM. This model may be useful in studying therapies relevant to perinatally-acquired CMV infections in infants. MWM studies of pups with congenital GPCMV infection would also be useful in evaluating vaccine strategies targeting prevention of the sequelae of congenital HCMV infection.

Supplementary Material

Refer to Web version on PubMed Central for supplementary material.

ACKNOWLEDGMENTS

We would like to thank Dr. Thomas Pengo, for his assistance with the use of the Imaris software and Steve Ricchio, who helped us to obtain the confocal images. Supported by NIH HD079918, HD098866, and NS038836.

Statement of Financial Support: Supported by NIH Grants HD079918, HD098866 and NS038836.

REFERENCES

1. Cheeran MC, Lokensgard JR, Schleiss MR. Neuropathogenesis of congenital cytomegalovirus infection: disease mechanisms and prospects for intervention. Clin Microbiol Rev 2009;22:99–126. [PubMed: 19136436]
2. Teissier N et al. Cytomegalovirus-induced brain malformations in fetuses. J Neuropathol Exp Neurol 2014;73:143–58. [PubMed: 24423639]
3. Gabrielli L et al. Congenital cytomegalovirus infection: patterns of fetal brain damage. Clin Microbiol Infect 2012;18:E419–27. [PubMed: 22882294]
4. Lanzieri TM et al. Long-term outcomes of children with symptomatic congenital cytomegalovirus disease. J Perinatol 2017;37:875–80. [PubMed: 28383538]
5. Dollard SC, Grosse SD, Ross DS. New estimates of the prevalence of neurological and sensory sequelae and mortality associated with congenital cytomegalovirus infection. Rev Med Virol 2007;17:355–63. [PubMed: 17542052]
6. Weimer KED, Kelly MS, Permar SR, Clark RH, Greenberg RG. Association of adverse hearing, growth, and discharge age outcomes with postnatal cytomegalovirus infection in infants with very low birth weight. JAMA Pediatr 2019; doi: 10.1001/jamapediatrics.2019.4532, PMID: 31790557.

7. Schleiss MR. Breast milk-acquired cytomegalovirus in premature infants: uncertain consequences and unsolved biological questions. JAMA Pediatr 2019; doi: 10.1001/jamapediatrics.2019.4538, PMID: 31790538.
8. Schleiss MR. Nonprimate models of congenital cytomegalovirus (CMV) infection: gaining insight into pathogenesis and prevention of disease in newborns. ILAR J 2006;47:65–72. [PubMed: 16391432]
9. Bravo FJ, Bourne N, Schleiss MR, Bernstein DI. An animal model of neonatal cytomegalovirus infection. Antiviral Res 2003;60:41–9. [PubMed: 14516920]
10. Tsutsui Y, Kosugi I, Kawasaki H. Neuropathogenesis in cytomegalovirus infection: indication of the mechanisms using mouse models. Rev Med Virol 2005;15:327–45. [PubMed: 16100703]
11. Slavuljica I et al. Immunobiology of congenital cytomegalovirus infection of the central nervous system—the murine cytomegalovirus model. Cell Mol Immunol 2015;12:180–91. [PubMed: 25042632]
12. Koontz T et al. Altered development of the brain after focal herpesvirus infection of the central nervous system. J Exp Med 2008;205:423–35. [PubMed: 18268036]
13. Brizić I et al. CD4 T cells are required for maintenance of CD8 TRM cells and virus control in the brain of MCMV-infected newborn mice. Med Microbiol Immunol 2019;208:487–494. [PubMed: 30923899]
14. Sung CYW et al. Virus-induced cochlear inflammation in newborn mice alters auditory function. JCI Insight 2019;4(17).
15. Ikuta K et al. Restricted infection of murine cytomegalovirus (MCMV) in neonatal mice with MCMV-induced sensorineural hearing loss. J Clin Virol 2015;69:138–45. [PubMed: 26209396]
16. Morris RGM. Spatial localization does not require the presence of local cues. Learn Motiv 1981;12:239–60.
17. D'Hooge R, De Deyn PP. Applications of the Morris water maze in the study of learning and memory. Brain Res Brain Res Rev 2001;36:60–90. [PubMed: 11516773]
18. Armien AG et al. Chronic cortical and subcortical pathology with associated neurological deficits ensuing experimental herpes encephalitis. Brain Pathol 2010;20:738–50. [PubMed: 20002440]
19. Buenz EJ, Rodriguez M, Howe CL. Disrupted spatial memory is a consequence of picornavirus infection. Neurobiol Dis 2006;24:266–73. [PubMed: 16919964]
20. Byrnes ML, Richardson DP, Brien JF, Reynolds JN, Dringenberg HC. Spatial acquisition in the Morris water maze and hippocampal long-term potentiation in the adult guinea pig following brain growth spurt--prenatal ethanol exposure. Neurotoxicol Teratol 2004;26:543–51. [PubMed: 15203176]
21. McAdam TD, Brien JF, Reynolds JN, Dringenberg HC. Altered water-maze search behavior in adult guinea pigs following chronic prenatal ethanol exposure: lack of mitigation by postnatal fluoxetine treatment. Behav Brain Res 2008;191:202–9. [PubMed: 18455245]
22. Fiset CRF, Surette ME, Fiset S. Prenatal iron deficiency in guinea pigs increases locomotor activity but does not influence learning and memory. PLoS One 2015;10.
23. LeBlanc CP, Fiset S, Surette ME, Turgeon O'Brien H, Rioux FM. Maternal iron deficiency alters essential fatty acid and eicosanoid metabolism and increases locomotion in adult guinea pig offspring. J Nutr 2009;139:1653–9. [PubMed: 19640965]
24. Mamczarz J et al. Spatial learning impairment in prepubertal guinea pigs prenatally exposed to the organophosphorus pesticide chlorpyrifos: Toxicological implications. Neurotoxicology 2016;56:17–28. [PubMed: 27296654]
25. McVoy MA et al. Repair of a mutation disrupting the guinea pig cytomegalovirus pentameric complex acquired during fibroblast passage restores pathogenesis in immune-suppressed guinea pigs and in the context of congenital infection. J Virol 2016; 90:7715–27. [PubMed: 27307567]
26. Bierle CJ, Anderholm KM, Wang JB, McVoy MA, Schleiss MR. Targeted mutagenesis of guinea pig cytomegalovirus using CRISPR/Cas9-mediated gene editing. J Virol 2016;90:6989–6998. [PubMed: 27226370]
27. Booss J, Winkler SR, Griffith BP, Kim JH. Viremia and glial nodule encephalitis after experimental systemic cytomegalovirus infection. Lab Invest 1989;61:644–9. [PubMed: 2557488]

28. Swanson EC et al. Comparison of monovalent glycoprotein B with bivalent gB/pp65 (GP83) vaccine for congenital cytomegalovirus infection in a guinea pig model: Inclusion of GP83 reduces gB antibody response but both vaccine approaches provide equivalent protection against pup mortality. Vaccine 2015;33:4013–8. [PubMed: 26079615]
29. Espinoza JA et al. Impaired learning resulting from respiratory syncytial virus infection. Proc Natl Acad Sci USA 2013;110:9112–7. [PubMed: 23650398]
30. Jurgens HA, Amancherla K, Johnson RW. Influenza infection induces neuroinflammation, alters hippocampal neuron morphology, and impairs cognition in adult mice. J Neurosci 2012;32:3958–68. [PubMed: 22442063]
31. Chen J et al. Long-term impact of intrauterine MCMV infection on development of offspring nervous system. J Huazhong Univ Sci Technolog Med Sci 2011;31:371–5. [PubMed: 21671180]
32. Lokensgard JR et al. Chronic reactive gliosis following regulatory T cell depletion during acute MCMV encephalitis. Glia 2015;63:1982–1996. [PubMed: 26041050]
33. Dringenberg HC, Richardson DP, Brien JF, Reynolds JN. Spatial learning in the guinea pig: cued versus non-cued learning, sex differences, and comparison with rats. Behav Brain Res 2001;124:97–101. [PubMed: 11423170]
34. Booss J, Dann PR, Griffith BP, Kim JH. Glial nodule encephalitis in the guinea pig: serial observations following cytomegalovirus infection. Acta Neuropathol 1988;75:465–73. [PubMed: 2837038]
35. Griffith BP, Lucia HL, Hsiung GD. Brain and visceral involvement during congenital cytomegalovirus infection of guinea pigs. Pediatr Res 1982;16:455–9. [PubMed: 6285263]
36. Bantug GR et al. CD8+ T lymphocytes control murine cytomegalovirus replication in the central nervous system of newborn animals. J Immunol 2008;181:2111–23. [PubMed: 18641350]
37. Cekinović D et al. Passive immunization reduces murine cytomegalovirus-induced brain pathology in newborn mice. J Virol 2008;82:12172–80. [PubMed: 18842707]
38. Mutnal MB, Hu S, Lokensgard JR. Persistent humoral immune responses in the CNS limit recovery of reactivated murine cytomegalovirus. PLoS One 2012;7:e33143.

IMPACT

What is the key message of this article?

- CMV impairs neonatal neurocognition and memory in the setting of post-natal infection.
- The Morris water maze (MWM) can be used to examine memory and learning in a guinea pig model of neonatal CMV infection.
- CD4+ and CD8+ T cells infiltrate the brain following neonatal CMV challenge.

What does this add to the existing literature?

- This article demonstrates that the MWM can be used to evaluate memory and learning after neonatal GPCMV challenge.

What is the impact?

- The guinea pig can be used to examine central nervous system pathology caused by neonatal CMV infection and this attribute may facilitate the study of vaccines and antivirals.

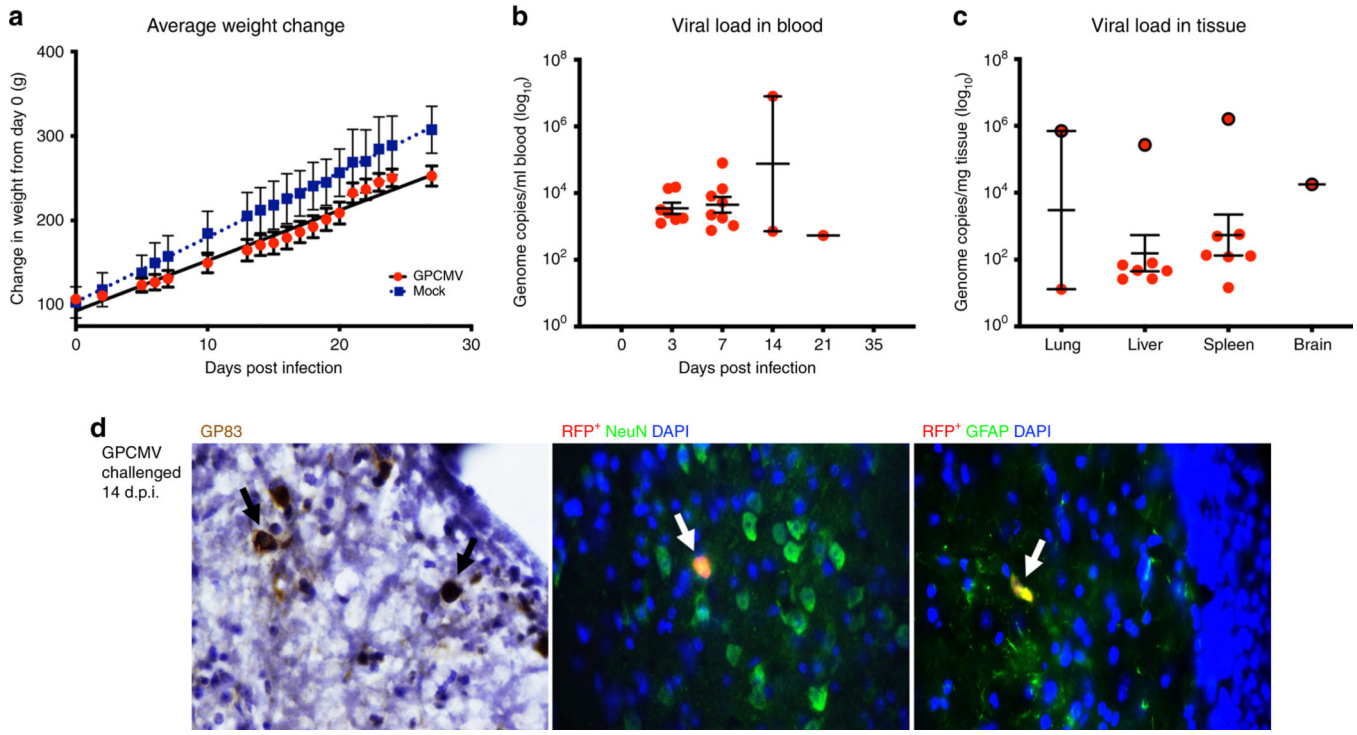

Figure 1:

Dissemination of GPCMV in a neonatal challenge model. **a)** Mean percentages of changes in weight demonstrating significantly slower weight gain ($p<0.05$) over time in challenged vs. sham-inoculated animals (mock). **b)** DNAemia was measured at the indicated time points post-infection. **c)** End-organ dissemination following examination of tissues at the time of necropsy (day 35), following completion of MWM studies. Viral DNA was noted in brain (1/8), lung (2/8), liver (7/8), and spleen (7/8). All data are from day 35 except for viral DNA detected in brain and visceral organs from the animal that necropsied at day 14 (closed circles); no viral DNA was noted in brains in animals necropsied at day 35. Data are represented as mean ± SEM. **d)** RFP+ (N13R10r129-RFP-infected) cells were observed in brain sections from animal described in section (c) above. Immunoperoxidase staining was performed using a GP83-specific rabbit moab (28) followed by secondary staining with HRP-conjugate horse anti-rabbit IgG (Vector Laboratories MP-7401) antibody and DAB substrate (SK 4105 Vector-Labs, brown cells), and this demonstrated GPCMV GP83 antigen in brain (left panel). Staining with either a rabbit anti-NeuN moab (middle panel) or a polyclonal rabbit anti-GFAP antibody (right panel) was also performed; secondary antibody, Alexa Fluor® 488 donkey anti-rabbit IgG (Table S1). This identified infected neurons and astrocytes, respectively (merged images, arrows) that were also expressing GPCMV antigen (as evidenced by RFP signal). All sections were counterstained with DAPI. 40X objective.

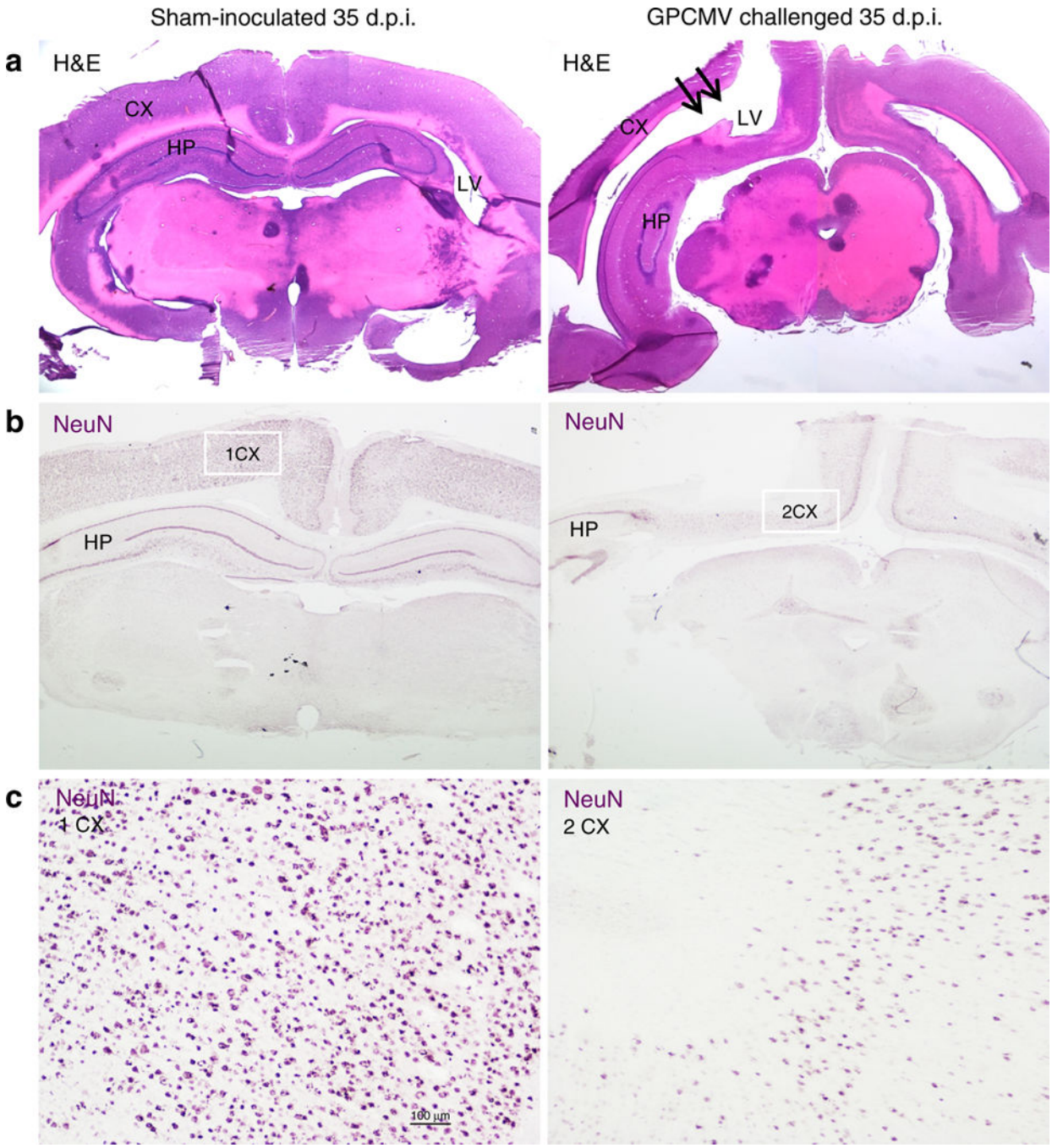

Figure 2:

Representative coronal brain sections from N13R10r129-RFP and sham-inoculated guinea pigs. **a)** Histological examination revealed extensive bilateral dilatation of lateral ventricles (LV) and reduced thickness of cerebral cortex (black arrows) in the challenged animal compared to the control. 10X magnification. **b)** Coronal sections (10X) demonstrating neuronal necrosis in N13R10r129-RFP challenged guinea pig (left panel) and control (right panel) at 35 days pi. Immunostaining was performed with rabbit NeuN moab and HRP-conjugate horse anti-rabbit IgG (Table S1), using VIP substrate (purple cells, SK 4605

Vector-Labs). Note the differences in intensity of NeuN immunoreactivity in uninfected control in the cerebral cortex (CX) and hippocampus (HP) regions compared to those in the infected animal. The panels in **(c)** represent higher magnification images of the indicated areas in panel **(b)**. In the un-infected control brain section, numerous NeuN-positive cells were observed. In contrast, fewer NeuN-positive cells were visualized in the brain section of the challenged guinea pig.

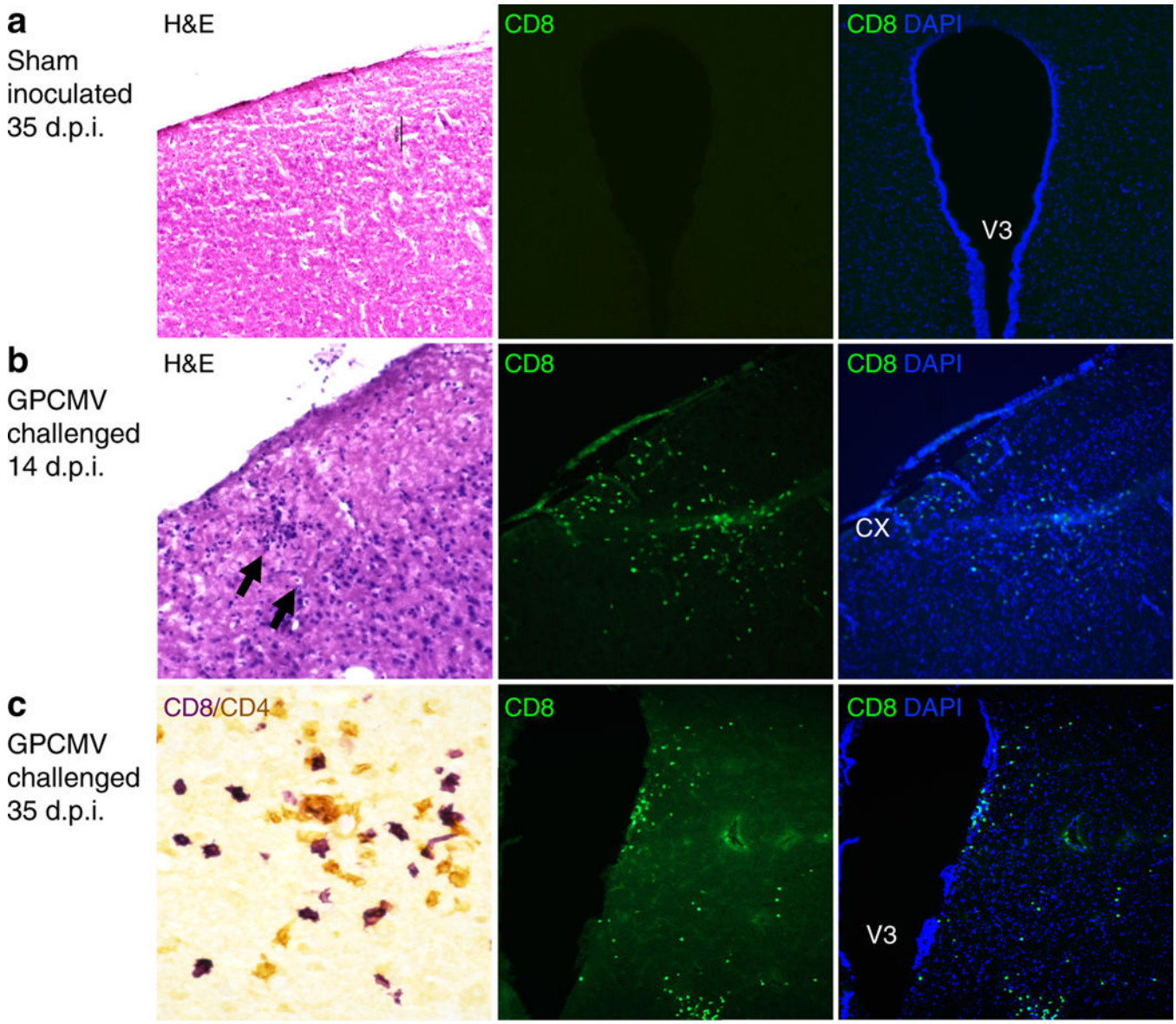

Figure 3:

Evidence of inflammatory cell infiltration in N13R10r129-RFP infected guinea pig brain. **a)** No $CD8^+$ T-lymphocytes were observed in sham-inoculated brains. **b)** Inflammatory cell infiltrates were localized in the brain cortical region (CX) and visualized by H&E (black arrows). T cells were visualized by staining with anti-guinea pig CD8+ moab and secondarily incubated with Alexa Fluor® 488 polyclonal anti-mouse IgG ab (green cells) at 14 days pi. **c)** T lymphocytes in brain sections were visualized in tissue obtained at 35 days pi by immunoperoxidase staining (double label): ImmPRESS anti-mouse IgG using CD4+ moab with DAB (brown cells) substrate, and ImmPRESS anti-mouse IgG using CD8+ moab with VIP (purple cells) substrate. CD8+ cells were also visualized in day 35 tissue using CD8+ moab (middle panel, CD8+; right panel, IFL with DAPI). Focal aggregates of CD8+ T-lymphocytes were localized around the region of the 3rd ventricle (V3). 10X objective

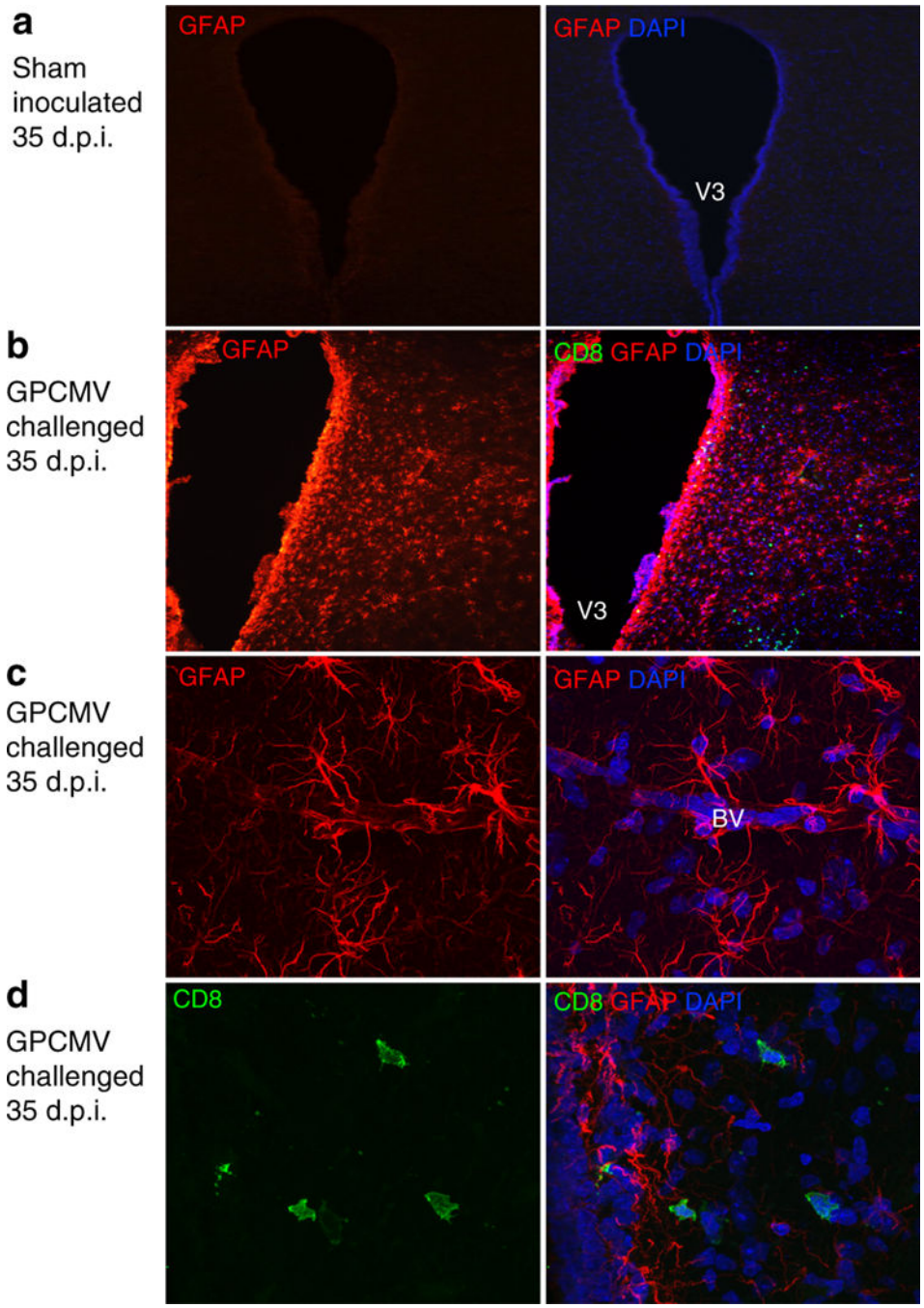

Figure 4:

Evidence of astrocyte activation and persistent chronic inflammation in N13R10r129-RFP-infected guinea pig (35 days pi) compared to uninfected control. **a, c)** Brain sections from infected and control animals were stained with polyclonal rabbit GFAP astrocyte marker antibody Z0334 (red cells) and Alexa Fluor® 594 donkey anti-rabbit secondary ab. Note the strongly positive GFAP-staining astrocytes with multiple elongated cell processes in tissue from infected animals in contrast to sham-inoculated animals. Confocal microscopy fluorescence of dense accumulation of GFAP+ end-feet and processes of reactive astrocytes

wrapping around blood vessels (BV) is noted. Note the dense staining of the enlarged cell bodies and the highlighted cell processes. **b, d)** In addition to GFAP, anti-CD8+ antibody staining with secondary ab (AlexaFluor® 488 polyclonal anti-mouse, green cells) staining is shown, with sections counterstained with DAPI. A reactive phenotype was visualized around the ventricular region (V3) and focal aggregates of CD8+ T-lymphocytes were noted around these reactive areas. CD8+ cells are associated with a prominent reactive astrogliosis as shown. Panels a, b: 10x objective. Panels c, d: 100x objective.

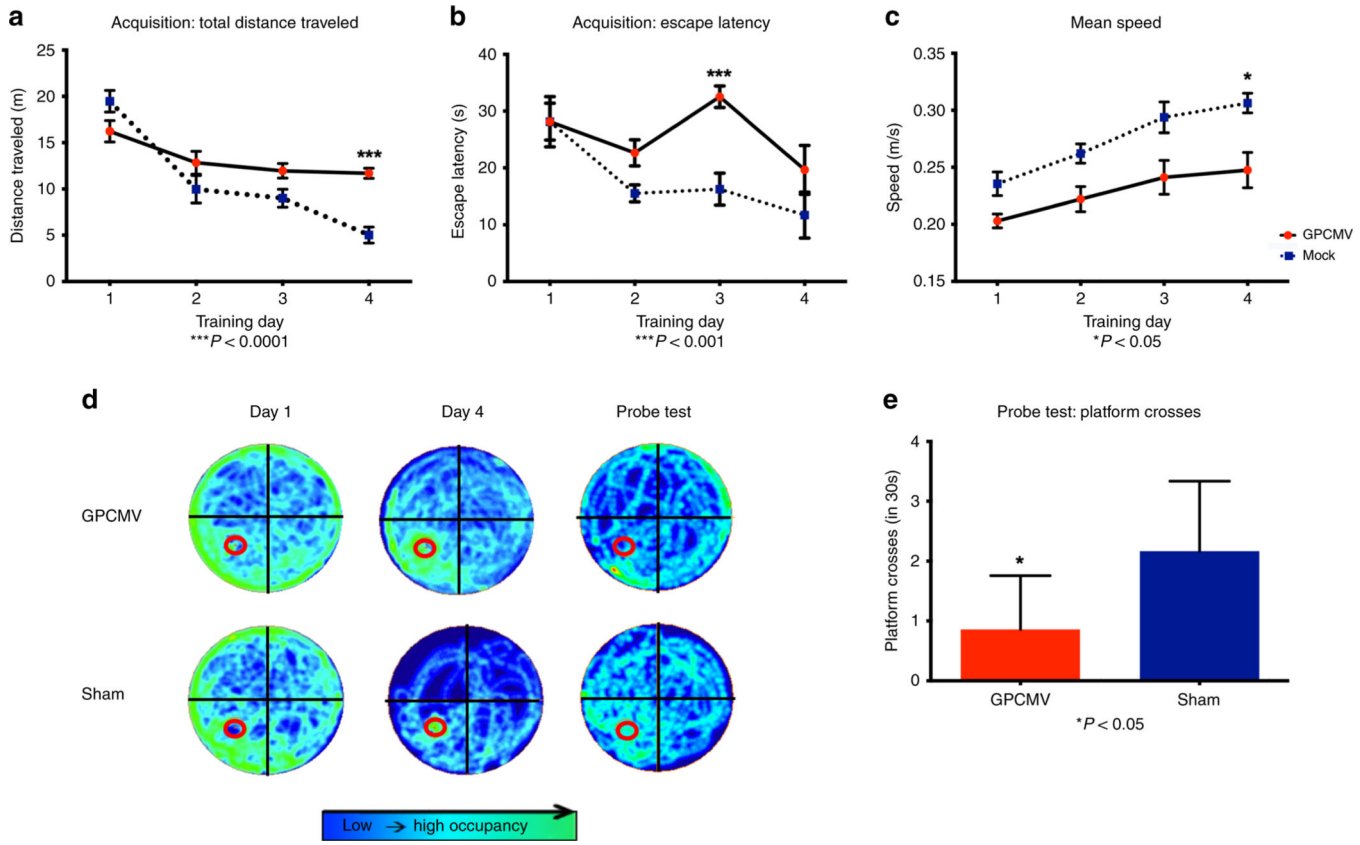

Figure 5:

Microglial cell reactivity and persistent chronic inflammation in N13R10r129-RFP challenged guinea pigs at 35 days pi. Brain sections were stained with rabbit moab to the microglial cell marker, Iba1 and an HRP-conjugated horse anti-rabbit IgG (MP-7401) with addition of VIP (purple) substrate. **a, b)** Positive microglial staining demonstrating a more reactive phenotype in challenged animals **(b)** in contrast with sham-inoculated animals **(a)**. **c)** Iba1^{+} staining demonstrating discrete microglial nodule formation dispersed throughout the brain in the same guinea pig shown in panel (b), necropsied at day 35. Left, low-power magnification (40X); right panels, enlargement of boxed regions designated in left panels.

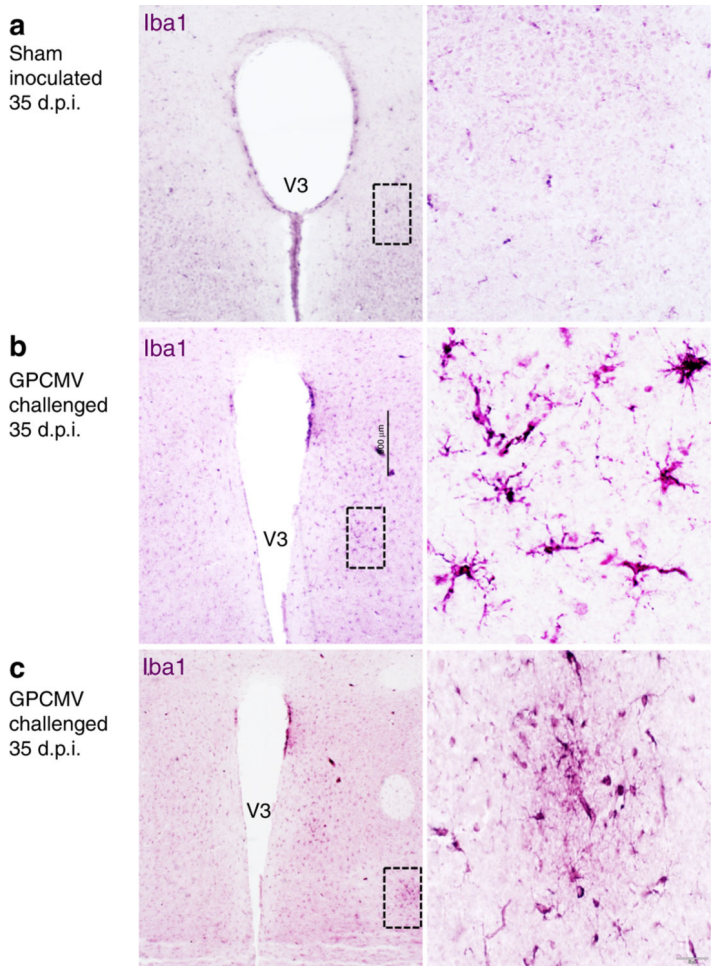

Figure 6:

Spatial learning and memory deficits in the challenged animals during the Morris water maze test. **a)** On the first day of acquisition training, there was no difference in total distance traveled between the sham-inoculated (mock) and the N13R10r129-RFP challenged group. By day 4, the challenged animals swam an average of 11.7 m compared to the 5.0 m traveled by the sham-inoculated group (***$p<0.0001$). **b)** Statistically significant decrease in the escape latency (time to find platform) in the sham-inoculated animal group during acquisition phase (***$p<0.001$). **c)** Graph shows swim speed of the N13R10r129-RFP challenged group versus sham-inoculated guinea pig. Statistical analysis showed a significant increase in the mean speed of the sham-inoculated group compared to challenge group (*$p<0.05$). **d)** Occupancy plots showing combined travel path of all animals on acquisition days 1 and 4 and during the probe phase on day 5. Sham-inoculated animals learned where the hidden platform was faster than N13R10r129-RFP challenged group. Red circle represents the hidden escape platform. Blue represent areas of low occupancy versus green regions representing areas of high occupancy. **e)** Reference memory tested during the probe phase. Challenged group performed fewer platform crosses (0.86) than the sham-inoculated animals (2.17; *$p<0.05$). Data are expressed as mean ± SEM.